

Identification of yrast high- K intrinsic states in ^{188}Os

V. Modamio,¹ A. Jungclaus,^{1,2} Zs. Podolyak,³ Y. Shi,⁴ F. R. Xu,⁴ A. Algora,⁵ D. Bazzacco,⁶ D. Escrig,² L. M. Fraile,⁷ S. Lenzi,⁶ N. Marginean,⁸ T. Martinez,⁹ D. R. Napoli,⁹ R. Schwengner,¹⁰ and C. A. Ur^{6,8}

¹*Departamento de Física Teórica C-XI, Universidad Autónoma de Madrid, E-28049 Madrid, Spain*

²*Instituto de Estructura de la Materia, CSIC, Serrano 113bis, E-28006 Madrid, Spain*

³*Department of Physics, University of Surrey, Guildford GU2 7XH, United Kingdom*

⁴*School of Physics, Peking University, Beijing 100871, People's Republic of China*

⁵*IFIC, CSIC/Universidad de Valencia, E-46071 Valencia, Spain*

⁶*Istituto Nazionale di Fisica Nucleare, Sezione di Padova, I-35131 Padova, Italy*

⁷*Universidad Complutense de Madrid, Madrid, Spain*

⁸*"Horia Hulubei" National Institute for Physics and Nuclear Engineering, Bucharest, Romania*

⁹*Istituto Nazionale di Fisica Nucleare, Laboratori Nazionali di Legnaro, I-35020 Legnaro, Italy*

¹⁰*Institut für Strahlenphysik, Forschungszentrum Dresden-Rossendorf, D-01314 Dresden, Germany*

(Received 23 September 2008; revised manuscript received 22 January 2009; published 17 February 2009)

The high-spin structure of the $Z = 76$ nucleus ^{188}Os has been studied using the incomplete fusion reaction $^7\text{Li} + ^{186}\text{W}$. A $K^\pi = 10^+$ band has been established up to spin (24^+) and its crossing with the ground-state band has been studied. In addition, intrinsic high- K states have been identified and on top of two of them, $K^\pi = 7^-$ and $K^\pi = 10^-$, regular bands have been observed. The $K^\pi = 16^+$ and $K^\pi = 18^+$ states are yrast whereas the $K^\pi = 14^+$ level lies only 33 keV above the yrast line and decays with a low reduced hindrance of $f_v < 1.3$ to the ground-state band ($\Delta K = 14$). The results are discussed by means of a systematic comparison with the even-even neighboring nucleus ^{186}Os . Configuration-constrained multiquasiparticle potential-energy-surface calculations have been performed to identify the configurations of multiquasiparticle states.

DOI: [10.1103/PhysRevC.79.024310](https://doi.org/10.1103/PhysRevC.79.024310)

PACS number(s): 21.10.Tg, 21.10.Ky, 21.60.Fw, 27.70.+q

I. INTRODUCTION

The Hf-W-Os nuclei in the mass 180 region are a rich playground for the study of high- K intrinsic states and their decay. In these nuclei high- Ω orbitals from both the $\nu i_{13/2}$ and the $\pi h_{11/2}$ shells are close to the Fermi surface and high- K ($K = \sum \Omega_n$) multiquasiparticle states can be formed at relatively low excitation energy [1]. In well-deformed, axially symmetric nuclei K is an approximately conserved quantum number and the decay of the high- K states is therefore governed by the selection rule $\Delta K \leq \mathcal{L}$ with \mathcal{L} being the multipole order of the γ ray emitted in the decay. Because of this selection rule, transitions from high- K intrinsic states to low- K collective bands such as the ground-state band are strongly hindered, leading in many cases to long lifetimes of the high- K states. However, there are different processes that may introduce K mixture and therefore erode the K selection rule. The Coriolis interaction changes the spin orientation and leads to $\Delta K = \pm 1$ mixing. For intrinsic states at high excitation energy statistical K mixing can substantially reduce the hindrance of K -forbidden transitions. Indeed, a strong correlation between the hindrance of K -forbidden transitions and the excitation energy of the decaying high- K state relative to a standard rotor has been observed and described within a statistical model based on level densities [2]. A third possible cause for a loss of hindrance are shape fluctuations involving the γ degree of freedom, which can couple states with $\Delta K = \pm 2$. In many cases all three described processes may cause a reduction of hindrances and it is not trivial to disentangle their relative contributions. The Os isotopes play an important role in this respect. It is known that, by adding more protons and neutrons

and thus leaving midshell, the prolate deformation decreases and the nuclear shapes become softer toward γ distortions. This trend, as evidenced by increasing energies within the ground-state band and decreasing energies of the $K^\pi = 2^+\gamma$ band, can be observed both moving from the Hf ($Z = 72$) to the Os ($Z = 76$) nuclei as well as within the Os isotopic chain going from ^{182}Os to ^{188}Os . Configuration-constrained potential-energy-surface (PES) calculations, which have been performed for several states in $^{182,184,186}\text{Os}$ [3–6], indicate that several of the observed high- K states have triaxial shape (e.g., the 25^+ isomer in ^{182}Os , the 21^+ and 22^- states in ^{184}Os , and the 18^+ and 28^+ levels in ^{186}Os). By extrapolating this trend it can be expected that ^{188}Os becomes triaxial at even lower rotational frequency. At the same time we observe that with increasing neutron number the intrinsic multiquasiparticle states tend to decrease in excitation energy with respect to the collective bands. Whereas in ^{182}Os all the observed intrinsic states lie well above the yrast line [7], already in ^{184}Os they are nearly touching the yrast line at spin $25\hbar$ [5,8]. Finally, in ^{186}Os the $K^\pi = 18^+$ four-quasiparticle state is yrast by 10 keV and many other multiquasiparticle states lie just above the yrast line [5,8].

The main aim of the present work has been to identify high- K multiquasiparticle yrast states at even lower spin in ^{188}Os and to study their decay properties. For yrast states statistical K mixing can be excluded and the observation of strongly reduced hindrances for the decay of high- K states can therefore be interpreted as evidence for triaxial shapes.

The article is organized as follows: In Sec. II details about the performed experiment as well as the data analysis procedure are given, and the resulting level scheme is presented

in Sec. III. The different structures of the excitation scheme are analyzed and discussed in comparison with neighboring Os isotopes as well as configuration-constrained multi-quasi-particle PES calculations in Sec. IV.

II. EXPERIMENT AND DATA PREPARATION

For many stable nuclei, which cannot be populated using heavy-ion-induced fusion-evaporation reactions with stable beams, knowledge of their structure at high spin is still scarce. In the chain of even-even Os isotopes for example, ^{184}Os can be reached using the $^{170}\text{Er}(^{18}\text{O},4n)$ [6] and $^{176}\text{Yb}(^{13}\text{C},5n)$ [3] reactions and ^{186}Os has been studied using a fusion-evaporation reaction induced by a radioactive ^{14}C beam [5,8]. Both nuclei have been extensively studied and in both cases complex excitation schemes have been obtained. ^{188}Os , in contrast, so far has only been studied up to intermediate spin using the $(\alpha,2n)$ reaction [9–11] and Coulomb excitation [12] and only states up to spin 12^+ have been identified. In our recent work on the heavy dysprosium isotopes $^{159-163}\text{Dy}$ [13,14] we have demonstrated that the incomplete fusion reaction induced by a ^7Li beam is a very valuable tool for populating stable neutron-rich nuclei up to high angular momentum (28^+ in ^{162}Dy [13]). In the present work we therefore employed the $^7\text{Li} + ^{186}\text{W}$ reaction to populate ^{188}Os via the $(^7\text{Li},p4n)$, $(^7\text{Li},d3n)$, and $(^7\text{Li},t2n)$ channels. The ^7Li beam at an energy of 59 MeV was provided by the XTU tandem accelerator of the Laboratori Nazionali di Legnaro and was directed on a 12 mg/cm² thick ^{186}W target. An excitation function was measured at beam energies of 51, 53, 56, and 59 MeV to choose the best conditions for the production of ^{188}Os . The γ radiation was detected in the 40 Compton-suppressed Ge detectors of the GASP array and the 80-crystal BGO calorimeter. Detection of charged particles was done using the Si ball ISIS, consisting of 40 ΔE - E telescopes arranged in the same geometry as the Ge crystals (i.e., in seven rings with $\theta = 35^\circ, 59^\circ, 72^\circ, 90^\circ, 108^\circ, 121^\circ,$ and 145° with respect to the beam axis). All events with at least three coincident γ rays in the Ge detectors or two γ rays in the Ge plus one particle detected in the Si ball were recorded on tape with the additional condition that the γ multiplicity in the BGO ball was three or higher. Time distributions of the γ rays were measured in a time window of 200 ns with respect to the prompt time signal of the BGO crystals. From these events, $\gamma\gamma$ matrices as well as $\gamma\gamma\gamma$ cubes were produced, both without time condition and requiring a prompt coincidence. For the latter, two-dimensional gates on the prompt region in the energy-time matrices of all 40 Ge detectors have been applied individually. Figure 1(a) shows the projection of the prompt $\gamma\gamma$ matrix without any particle condition. From this projection we see that the two nuclei $^{187,188}\text{Ir}$ [15,16] are most strongly populated in the reaction via the $6n$ and $5n$ channels, respectively. However, by requiring the detection of at least one proton, deuteron, or triton in coincidence with the γ rays, the Ir isotopes can be eliminated and the projections of these $\gamma\gamma p$, $\gamma\gamma d$, and $\gamma\gamma t$ matrices contain only γ rays from the decay of the $^{187-189}\text{Os}$ isotopes [see Figs. 1(b)–1(d)]. A very nice feature of the incomplete fusion reaction is

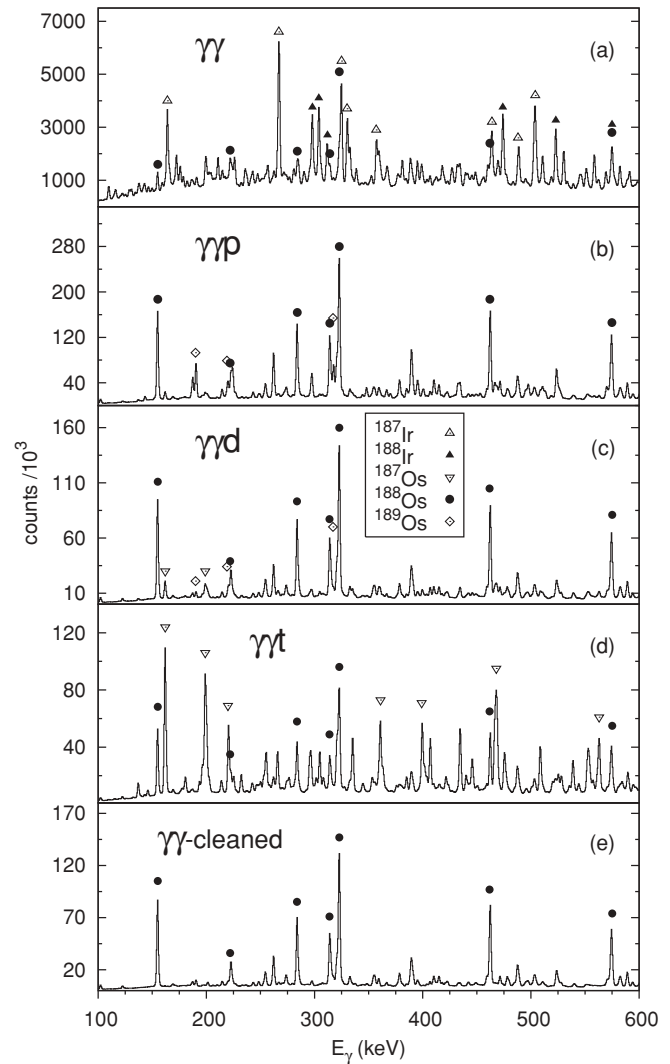


FIG. 1. Projections of the $\gamma\gamma$ matrices (a) without particle condition and requiring either a proton (b), a deuteron (c), or a triton (d) coincidence. The projection of the clean ^{188}Os matrix is shown in (e). Peaks corresponding to transitions in ^{187}Ir , ^{188}Ir , ^{187}Os , ^{188}Os , and ^{189}Os are labeled by symbols as indicated in the inset, respectively.

that the different final products are populated with different probabilities via the channels pxn , $d(x-1)n$, and $t(x-2)n$. For the lighter isotope ^{187}Os the triton channel is the most probable whereas the heavier ^{189}Os is mainly populated via the proton channel. Because of this property and the large particle detection efficiency of the ISIS ball, it is possible to produce rather clean matrices for each isotope. In the case of ^{188}Os , fractions of the $\gamma\gamma p$ and $\gamma\gamma t$ matrices have been subtracted from the $d\gamma\gamma$ matrix, resulting in a clean ^{188}Os matrix as shown in Fig. 1(e). In this matrix, the intensity of the strongest contaminating line from $^{187,189}\text{Os}$ amounts to less than 1% of the intensity of the 323-keV peak in ^{188}Os . The construction of the level scheme discussed in the next section is mainly based on the analysis of this clean ^{188}Os matrix and the ungated $\gamma\gamma\gamma$ cube.

To determine γ -ray multipole orders, directional angular correlation ratios from oriented states (DCO) have been measured. For this purpose, $\gamma\gamma$ events with one γ ray detected in one of the 12 detectors at 35° and 145° and the other detected in one of the 8 detectors at 72° and 108° relative to the beam direction were sorted into an asymmetric coincidence matrix. A second DCO matrix was built by requiring a coincidence with either a proton or a deuteron. Then, by using a coincidence gate on a stretched quadrupole transition γ_{gate} , the ratio

$$R_{\text{DCO}} = \frac{I_\gamma(\text{at } \theta_1 | \gamma_{\text{gate}} \text{ at } \theta_2) \varepsilon_{\theta_2}(\gamma) \varepsilon_{\theta_1}(\gamma_{\text{gate}})}{I_\gamma(\text{at } \theta_2 | \gamma_{\text{gate}} \text{ at } \theta_1) \varepsilon_{\theta_1}(\gamma) \varepsilon_{\theta_2}(\gamma_{\text{gate}})}$$

is expected to be ≈ 1 for stretched quadrupole and ≈ 0.6 for pure dipole transitions ($\theta_1 = 35^\circ, 145^\circ, \theta_2 = 72^\circ, 108^\circ$). Here $\varepsilon_\theta(\gamma)$ are the relative efficiencies of the detectors positioned at an angle θ with respect to the beam at energy E_γ .

III. THE LEVEL SCHEME OF ^{188}Os

The level scheme of ^{188}Os has been extensively investigated in the 1970s by using the $(\alpha, 2n)$ reaction [9–11]. In these studies, the ground-state band has been established up to spin 12^+ , the γ band observed up to the 6^+ state, and a 4^+ level interpreted as the bandhead of the $K = 4$ two-phonon γ -vibrational band. At negative parity, intrinsic states with $I^\pi = 3^-, 5^-,$ and 7^- have been reported and for the 7^- state a lifetime of $\tau = 20.2(14)$ ns has been measured by Shibata *et al.* [17]. In this article we present a considerable extension of the level scheme of ^{188}Os . More than 90γ transitions have been observed for the first time and placed in the excitation scheme, including an extension of the ground-state band up to spin 16^+ and of the γ band up to spin 13^+ . In addition, three new bands with $K^\pi = 7^-, K^\pi = 10^-,$ and $K^\pi = 10^+$ have been established and a new complex irregular structure formed by multiquasiparticle states has been observed.

Figure 2 shows the level scheme deduced in the present work. Spin and parity assignments have been made mainly based on measured DCO ratios and electron conversion coefficients. The energies and relative intensities of all observed transitions together with their placement in the level scheme and the experimental DCO ratios are summarized in Table I. In the following sections the main structures of the excitation scheme of ^{188}Os will be discussed in detail.

A. The ground-state band and the $K^\pi = 10^+$ band

The ground-state band (gsb) had been established up to the 12^+ state in Ref. [10]. In a recent experiment using deep inelastic reactions additional γ rays of 615, 523, 262, 395, 471, and 495 keV have been observed [18] and placed as a cascade feeding the 12^+ level from a 21^+ state. Figure 3 shows a coincidence spectrum with a gate on the 686-keV $12^+ \rightarrow 10^+$ transition projected from the clean ^{188}Os matrix. The strongest lines at 655, 575, 462, 323, and 155 keV correspond to the $E2$ cascade from the 10^+ state to the ground state and a series of additional lines is visible including the first three transitions observed in Ref. [18]. However, the relative intensities of 182(4), 136(3), and 183(5) for the 616-, 524-, and 262-keV

TABLE I. Energies, intensities, DCO ratios, initial state excitation energy, and initial and final state spins of γ transitions in the level scheme in ^{188}Os . The intensities are not corrected for internal conversion.

E_γ (keV)	I_γ	R_{DCO}	E_i (keV)	I_i^π	I_f^π
89.2	74(4)		2144.9	10^-	9^-
102.4	252(6)		1771.6	7^-	5^-
155.2	1000(20)	0.83(9)	155.2	2^+	0^+
223.0	264(7)	0.41(5)	1994.6	8^-	7^-
236.4	14(1)		1516.0	5^+	4^+
243.8	67(2)	2(1)	1669.2	5^-	6^+
248.5	58(1)		2243.1	9^-	8^-
254.5	198(8)	0.5(1)	1669.2	5^-	3^-
254.9		0.9(2)	2813.8	11^+	10^+
262.3	183(5)	1.00(12)	3734.6	16^+	14^+
267.0	49(2)		3084.0		
270.2	17(1)		3084.0		11^+
274.4	86(2)	0.5(2)	3255.8	(13^+)	12^+
275.1	16(1)		2734.2	12^-	11^-
279.8	11(2)		2522.9	10^-	9^-
284.1	762(17)	0.85(6)	2055.7	9^-	7^-
292.8	3(1)		3353.2	14^-	13^-
294.1	6(1)		2817.0		10^-
314.2	437(12)	0.28(2)	2459.1	11^-	10^-
316.0	93(6)	0.25(4)	2817.0		(11^-)
320.4	199(7)		3734.6	16^+	15^-
320.5		0.94(9)	3414.2	15^-	13^-
323.1	1341(32)	0.97(7)	478.3	4^+	2^+
326.2	49(1)		3060.4	13^-	12^-
332.7	91(3)	1.4(3)	966.0	4^+	2^+
333.7	10(1)		3417.7		
353.8	68(2)	0.9(2)	3414.2	15^-	13^-
354.6			3826.9		14^+
356.1	87(2)	0.40(6)	2501.0	(11^-)	10^-
356.8			3796.0	15^+	14^+
359.5	79(2)	0.29(6)	3093.7	13^-	12^-
366.7	23(1)		4193.6		
378.6	114(3)	0.62(5)	3472.3	14^+	13^-
383.8			5033.8	(19^-)	18^+
388.7			3205.7		
389.6	532(15)	0.51(8)	1669.2	5^-	4^+
391.4	140(6)	1.25(15)	1181.6	5^+	3^+
391.6			4650.0		18^+
395.4	36(3)	0.86(13)	5125.4	21	19
410.4	88(2)	0.34(9)	2869.5	(12^-)	11^-
414.1			4564.0		
415.3	77(2)	0.21(3)	4149.9		16^+
415.5			3621.1		
420.7	27(1)		3290.2		(12^-)
423.1	30(2)		2981.4	12^+	10^+
432.5	5(1)		3722.7		
442.0	44(1)		3255.8	13^+	11^+
448.7	55(4)		1414.7	3^-	4^+
458.0			3439.2	14^+	12^+
459.4	115(5)	0.47(15)	1425.4	6^+	4^+
462.4	860(20)	0.99(5)	940.7	6^+	4^+
462.7			4185.4		
471.5	51(2)		2243.1	(9^-)	7^-
471.6		0.34(7)	4730.0	19	18^+

TABLE I. (*Continued.*)

E_γ (keV)	I_γ	R_{DCO}	E_i (keV)	I_i^π	I_f^π
478.1	172(5)	0.8(2)	633.3	2 ⁺	2 ⁺
479.5	45(2)	0.26(8)	4391.1		
484.7	37(1)	6	1425.4	6 ⁺	6 ⁺
487.6	429(9)		1669.2	5 ⁻	5 ⁺
487.7		0.63(12)	966.0	4 ⁺	4 ⁺
489.4	151(4)		1279.6	4 ⁺	3 ⁺
489.5		1.06(15)	6607.7		
495.3	19(1)		5620.7		21
497.4	29(2)		3911.6		15 ⁻
497.5			6118.2		
503.2	177(6)	0.60(11)	2558.9	10 ⁺	9 ⁻
503.5			1685.1	7 ⁺	5 ⁺
523.8	136(3)	0.96(12)	4258.4	18 ⁺	16 ⁺
524.5		0.99(15)	5033.8	19 ⁻	17 ⁻
525.8	48(2)	1.0(3)	3965.0	16 ⁺	14 ⁺
528.3	40(1)		2522.9	10 ⁻	8 ⁻
540.2	18(1)		3796.0	15 ⁺	13 ⁺
550.0	16(1)		1516.0	5 ⁺	4 ⁺
571.1	70(4)	0.9(2)	1996.5	8 ⁺	6 ⁺
573.9		0.7(2)	2817.0		9 ⁻
574.7	558(14)	1.16(7)	1515.4	8 ⁺	6 ⁺
582.4	46(3)	1.21(6)	3439.2	14 ⁺	12 ⁺
583.0	77(4)	1.3(3)	3084.0		(11 ⁻)
589.3	175(4)	1.02(9)	2734.2	12 ⁻	10 ⁻
594.1		1.06(2)	2279.2	9 ⁺	7 ⁺
601.3	95(3)	0.9(1)	3060.4	13 ⁻	11 ⁻
607.3		0.6(2)	4572.3	18 ⁺	16 ⁺
615.5	182(4)	1.05(9)	3472.3	14 ⁺	12 ⁺
619.0	53(3)	1.1(3)	3353.2	14 ⁻	12 ⁻
621.2	25(2)		3144.1		10 ⁻
624.5	93(3)		1414.7	3 ⁻	3 ⁺
629.2	18(3)	1.2(3)	4887.6		18 ⁺
633.3	262(9)	0.9(3)	633.3	2 ⁺	0 ⁺
634.6	653(18)	0.81(14)	3093.7	13 ⁻	11 ⁻
635.0			790.2	3 ⁺	2 ⁺
642.7	33(2)	0.9(3)	5033.8	19 ⁻	17 ⁻
646.3	339(8)	0.74(15)	1279.6	4 ⁺	2 ⁺
654.0	33(2)	1.0(4)	2933.2	11 ⁺	9 ⁺
655.3	431(12)	1.03(8)	2170.7	10 ⁺	8 ⁺
659.1	36(2)	1.4(7)	2655.6	10 ⁺	8 ⁺
668.0	20(1)	1.0(5)	3601.2	13 ⁺	11 ⁺
670.8	50(2)	1.6(4)	3731.2		13 ⁻
673.9	16(1)		4237.0	(16 ⁺)	14 ⁺
681.7	9(2)		3825.8		
686.1	325(7)	1.01(7)	2856.8	12 ⁺	10 ⁺
693.0	36(4)		5177.8		
694.4	33(3)	1.1(2)	4429.0		16 ⁺
695.4	12(3)		4521.2		
695.7			5268.0	(20 ⁺)	18 ⁺
703.2	365(9)	0.48(14)	1669.2	5 ⁻	4 ⁺
703.3		0.78(14)	1181.6	5 ⁺	4 ⁺
706.3	53(3)		3563.1	14 ⁺	12 ⁺
707.5	18(2)	1.1(2)	3441.7		12 ⁻
714.4	6(2)	1.2(4)	3370.0	12 ⁺	10 ⁺
725.8	28(1)	0.9(2)	1516.0	5 ⁺	3 ⁺
728.5	236(5)	0.8(2)	1669.2	5 ⁻	6 ⁺
739.8	21(1)		4847.3		16 ⁻

TABLE I. (*Continued.*)

E_γ (keV)	I_γ	R_{DCO}	E_i (keV)	I_i^π	I_f^π
745.0	15(2)		1685.1	7 ⁺	6 ⁺
753.6	16(1)		4484.8		
754.3		0.8(2)	4107.5	16 ⁻	14 ⁻
764.4	9(1)		6032.4	(22 ⁺)	(20 ⁺)
775.4	15(1)	0.85(15)	5033.8	19 ⁻	18 ⁺
783.9	19(1)	0.8(2)	3640.7		12 ⁺
810.7	145(3)		2981.4	12 ⁺	10 ⁺
810.8		1.3(3)	966.0	4 ⁺	2 ⁺
830.7	29(3)		1771.6	7 ⁻	6 ⁺
878.6			6911.0	(24 ⁺)	(22 ⁺)
910.4	9(1)		3767.2		12 ⁺
913.3	26(1)		3084.0		10 ⁺
933.0	9(1)		4286.2		14 ⁻
936.4	20(1)		1414.7	3 ⁻	4 ⁺
947.1	12(1)		1425.4	6 ⁺	4 ⁺
976.9	13(1)	1.0(4)	4391.1	(17 ⁻)	15 ⁻
1095.1	36(2)	1.1(2)	4509.3	(17 ⁻)	15 ⁻
1190.9	50(2)		1669.2	5 ⁻	4 ⁺

lines seem to contradict the order in which they are placed in Ref. [18]. A further careful analysis of all coincidence relations lead us to place the 616-keV transition directly feeding the 12⁺ member of the gsb and the 262- and 524-keV transitions connecting multi-quasiparticle states above (see the following). The next strongest line observed in coincidence with the 686-keV transition (see Fig. 3), namely the one at 582 keV, is a second direct feeder of the 12⁺ state at 2857 keV and connects the newly proposed $K^\pi = 10^+$ band to the gsb. A double gate on this 582-keV transition and one of the 686-, 655-, and 575-keV members of the gsb in the prompt $\gamma\gamma\gamma$ cube is shown in Fig. 4(a). Besides the gsb members, γ rays with 526, 607, and 696 keV are observed forming a regular sequence on top of the 14⁺ 3439-keV level. Two more transitions with 764 and 879 keV belonging to this band become visible when more coincidence spectra are summed. Two states at 2559 and 2981 keV decaying by γ rays of 503 and 811 keV to a 9⁻ state at 2056 keV and the 10⁺ member of the gsb, respectively, have been assigned as the bandhead and the 12⁺ member of the new $K^\pi = 10^+$ band. Coincidence spectra with gates on these 811- and 503-keV γ rays are shown in Figs. 4(b) and 4(c). In the 811-keV spectrum three lines at 274, 458, and 540 keV are observed in addition to the gsb transitions. Whereas the weak 458-keV line represents the in-band 14⁺ \rightarrow 12⁺ transition, the 274-keV line is feeding the 12⁺ state from the 13⁺ odd-spin band member. A similar observation is made in the 503-keV gate in which again the feeding from the odd-spin 11⁺ state via a 255-keV transition is stronger than the 422-keV feeding in-band transition. In this spectrum also the 442- and 540-keV $E215^+ \rightarrow 13^+ \rightarrow 11^+$ transitions as well as the most prominent γ rays from the decay of the 9⁻ state are observed. The spin of this newly observed band is unequivocally fixed on the basis of the measured DCO ratios of 0.60(11) for the 503-keV 10⁺ \rightarrow 9⁻ and 1.21(6) for the 582-keV 14⁺ \rightarrow 12⁺ transitions.

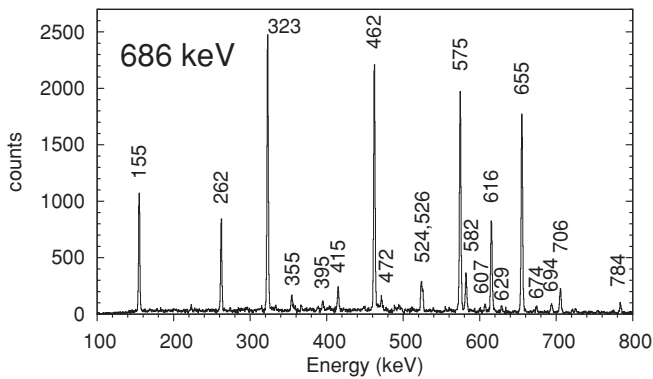


FIG. 3. Coincidence spectrum with gate on the 686-keV $12^+ \rightarrow 10^+$ member of the gsb in the clean ^{188}Os matrix.

B. Low-spin negative-parity states and the $K^\pi = 7^-$ band

Three negative-parity states with $I^\pi = 3^-, 5^-,$ and 7^- have been reported by Yates *et al.* [9]. In that work the 7^- state has been suggested to correspond to the isomeric state with a half-life of about 20 ns whose existence had been postulated by Yamazaki and Nishiyama [11] based on the observation of delayed interband transitions between the γ band and the gsb. This assignment was later confirmed by a direct measurement of the time distribution of the 102-keV $7^- \rightarrow 5^-$ transition leading to $\tau(7^-) = 20.2(14)$ ns [17]. Two more γ rays with 223 and 284 keV feeding the 7^- state have been observed in Refs. [9,17]. Based on the measured DCO ratios for these γ rays we propose spin values of (8^-) and 9^- for the states at 1995 and 2056 keV, respectively. On top of the isomeric 7^- state a band with two regular $E2$ sequences has been identified. The known 223-keV γ ray and new ones with 249, 280, and 294 keV are $M1$ transitions connecting the signature partners in the lower part of the band.

C. The $K^\pi = 10^-$ band

The by far strongest line observed in coincidence with the 284-keV $9^- \rightarrow 7^-$ transition is the one at 314 keV. A very careful coincidence analysis led to the establishment of another regular band with two parallel $E2$ sequences (601–671–754–693 keV and 589–619–754–740 keV) and again a number of $M1$ transitions (the strongest being the 314-keV transition) connecting the two signatures as in the case of the $K^\pi = 7^-$ band. Figure 5 shows the spectra in coincidence with the lowest $E2$ transitions within the two signatures, namely the 589- and 601-keV γ rays. In the spectrum gated on the 601-keV transition we observe that the intensity of the 314-keV line is higher than the sum of the intensities of the 284- and 223-keV lines although it should be the same considering the established decay scheme (see Fig. 2). Since these spectra were obtained by applying a prompt time condition the natural explanation of this observation is the existence of a nanosecond lifetime of either the 10^- or the 9^- state between the 314-keV and the parallel 284- and 223-keV transitions. In the insets in Fig. 5 a candidate for the isomeric transition, namely a 89-keV γ ray, is clearly observed in addition to the known 102-keV $7^- \rightarrow 5^-$ transition. The experimental conversion coefficient

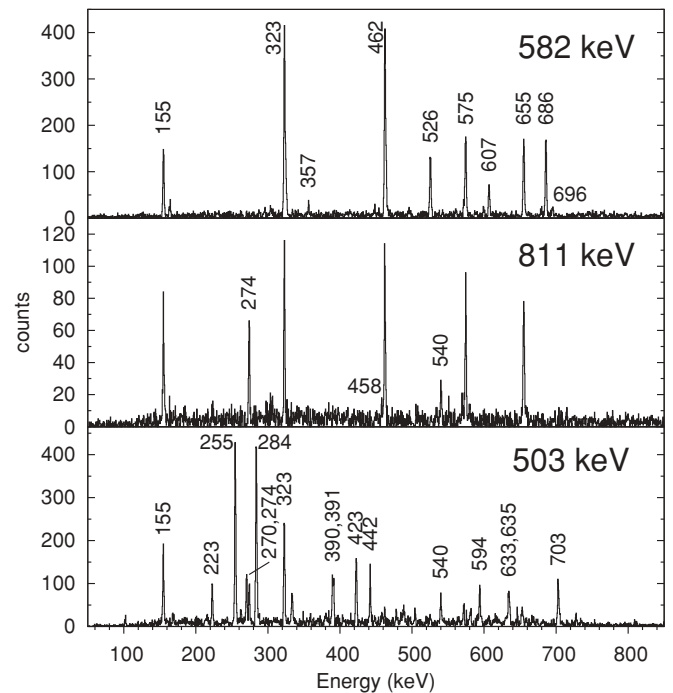


FIG. 4. Double-gated coincidence spectra with gates on (a) 582-keV and one of the 686-, 655-, or 575-keV transitions and on (b) 811-keV and one of the 686-, 655-, or 575-keV transitions; (c) single-gated coincidence spectrum with gate on the 503-keV transition.

[$\alpha = 13(1)$] deduced from the observed intensities favors $M1$ or $E2$ multipolarity for the 89-keV γ ray, limiting the possible spin values for the bandhead from which it decays to 10^- or 11^- . The value of 10^- has finally been fixed based on DCO ratios for transitions connecting positive-parity high-spin states to this new band (see the following discussion) such as the 354- and 360-keV transitions observed in coincidence with the 601- and 589-keV γ rays in Fig. 5. A direct proof that the 10^- is the isomeric state and not the 9^- level comes from the prompt coincidence spectrum with gate on the 503-keV $10^+ \rightarrow 9^-$ γ ray already presented in Fig. 4(c). In this spectrum

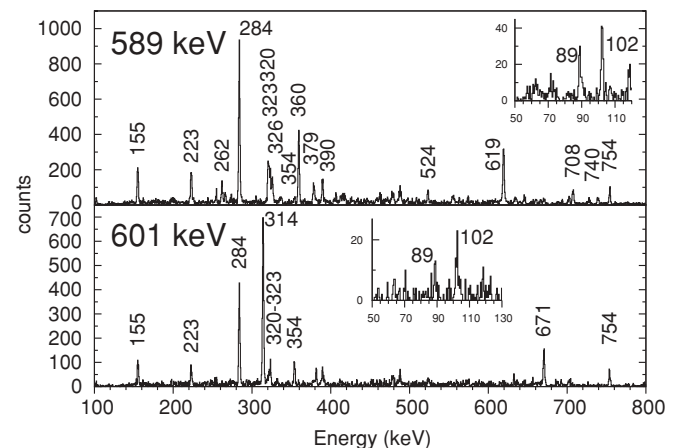


FIG. 5. Single-gated coincidence spectra with gate on the 589-keV (a) and 601-keV (b) transitions within the $K^\pi = 10^-$ band.

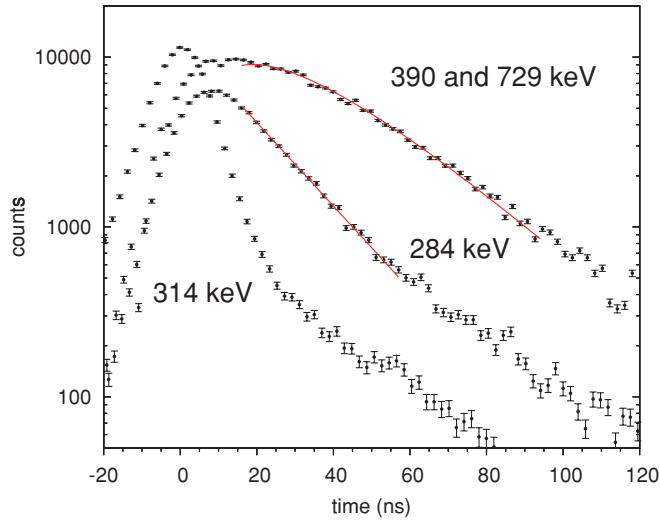


FIG. 6. (Color online) Time distributions observed for the 284-keV and the sum of the 390- and 729-keV γ rays in prompt coincidence with the 314-keV $11^- \rightarrow 10^-$ transition. Continuous lines represent the fits to the data points (see text for details).

the summed intensity of the two transitions feeding the 10^+ state (255 and 423 keV) is the same as the summed intensity of the 223- and 284-keV γ rays below the 9^- state. If the 9^- level would have the isomeric lifetime, the latter intensity should be reduced in the same way as just discussed for the 601-keV coincidence spectrum.

To determine the lifetime of the head of the $K^\pi = 10^-$ band at 2145 keV an energy-time matrix in prompt coincidence with the 314-keV transition feeding this state has been sorted. In this way the feeding path is well determined and the time distribution obtained for the 284-keV transition, which is shown in Fig. 6, can be directly assigned to the lifetime of the 10^- state. Fitting an exponential decay to the slope results in a lifetime of $\tau(10^-) = 17.7(2)$ ns. For reference the prompt time distribution of the 314-keV transition is included in Fig. 6, too. To determine the lifetime of the 7^- state the time distributions of the 390- and 729-keV γ rays decaying from the 5^- level have been used. Since a prompt gate on the 314-keV transition is applied, $\tau(7^-)$ can be determined from a fit of the function

$$N(t) = N_0 \frac{\lambda(10^-)\lambda(7^-)}{\lambda(7^-) - \lambda(10^-)} [e^{-t/\tau(10^-)} - e^{-t/\tau(7^-)}]$$

to the observed time distribution, by taking into account the known value of $\tau(10^-)$. We obtain $\tau(7^-) = 20.2(3)$ ns, in perfect agreement with the literature value of $\tau_{lit}(7^-) = 20.2(14)$ ns [17].

D. The four-quasiparticle states

As previously mentioned, in the coincidence spectrum gated on the 686-keV $12^+ \rightarrow 10^+$ member of the gsb (see Fig. 3) the strongest transitions feeding the 12^+ level are the ones with 616 and 262 keV with nearly the same intensity. The measured DCO ratios [1.05(9) and 1.00(12), respectively] identify both as $E2$ transitions and based on coincidence relations we place the 616-keV γ ray as directly feeding the

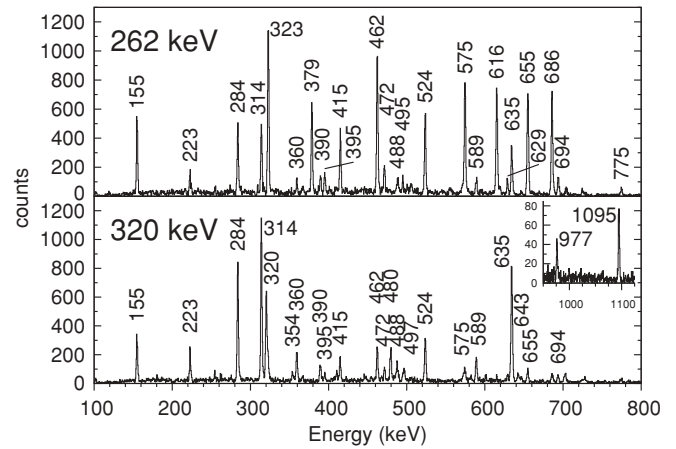


FIG. 7. Single-gated coincidence spectra with gate on the 262-keV $16^+ \rightarrow 14^+$ transition (a) and the 320-keV doublet (b).

12^+ gsb state from a 14^+ state at 3472 keV, only 33 keV above the yrast 14^+ state, and the 262-keV γ ray on top of it decaying from the 16^+ yrast state at 3735 keV. The spectrum observed in coincidence with this 262-keV transition is shown in Fig. 7(a). Besides the decay to the gsb via the 616-keV line, visible is a second decay branch of the 14^+ state via γ rays of 379 and 635 keV and 360 keV, respectively, to the 11^- and 12^- members of the $K^\pi = 10^-$ band. The 16^+ state at 3735 keV is mainly fed by a strong 524-keV transition. This γ ray together with the $16^+ \rightarrow 14^+$ transition of the $K^\pi = 10^+$ band forms a doublet in the 686-keV coincidence spectrum of Fig. 3, which probably led to the wrong ordering of the 616-, 262-, and 524-keV transitions in Ref. [18]. In addition to the 262-keV transition to the 14^+ level at 3472 keV, the 16^+ state decays in parallel via a 320- and 354-keV cascade to the 13^- member of the $K^\pi = 10^-$ band. It is this network of interconnecting transitions with the measured DCO ratios that allowed us to unequivocally fix the spin of the $K^\pi = 10^-$ band. The 320-keV line is a doublet, as is evident from Fig. 7(b), which shows its coincidence spectrum. In both the 262- and the 320-keV spectra, lines at 472, 395, and 495 keV are observed and placed as cascade feeding the 18^+ 4258-keV state. When more coincidence spectra are summed this sequence can tentatively be extended by two more transitions of 498 and 490 keV. As shown in the inset of Fig. 7(b), additional lines at higher energies are observed in coincidence with the 320-keV γ ray, namely at 977 and 1095 keV. These transitions belong to a structure connecting a 19^- state at 5034 keV to the (15^-) level at 3414 keV. The 19^- level also decays to the 18^+ state at 4258 keV via a 775-keV γ ray [compare Fig. 7(a)]. Both this 19^- state and a level at 4564 keV decaying by two 415-keV γ rays of nearly the same energy to the 16^+ state seem to be isomeric. Although the γ rays from their decays are observed with significant intensities it was not possible to identify transitions feeding these states.

IV. DISCUSSION

The new experimental results presented in this article allow us to extend the systematics of collective bands as

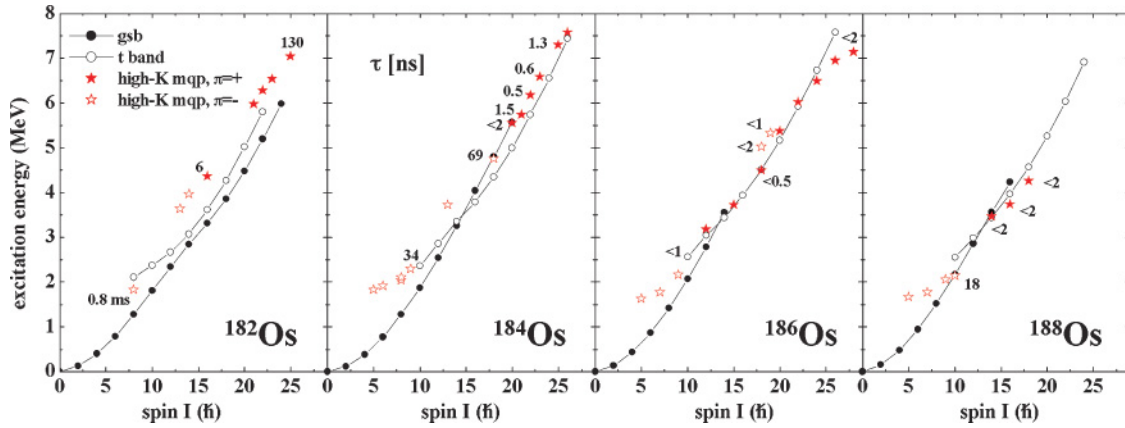


FIG. 8. (Color online) Yrast line and high- K multi-quasiparticle (mpq) states in the even-even nuclei $^{182-188}\text{Os}$.

well as intrinsic states in the even-even Os isotopes to the $N = 112$ isotope ^{188}Os . The systematics as shown in Fig. 8 for the four even-even isotopes $^{182-188}\text{Os}$ nicely illustrate the decrease in excitation energies of the intrinsic states relative to the collective bands with increasing neutron number. At the same time the lifetimes of these states decrease, indicating the importance of shape effects at lower and lower spin in the heavier Os nuclei.

Since the level scheme of ^{188}Os as established in the present work shows many similarities to the one of its lighter even-even neighbor ^{186}Os , we will start with a discussion of its properties in comparison to this nucleus. In the following sections the collective band structures and the intrinsic multi-quasiparticle states will be discussed in detail.

A. Ground-state band, $K^\pi = 10^+$ band, and γ band

The three collective bands observed in ^{186}Os and ^{188}Os , namely the ground-state band, the $K^\pi = 10^+$ band, and the γ band, show a very similar behavior in both nuclei as illustrated in Fig. 9. The transition energies within the gsb are somewhat larger in ^{188}Os , indicating a decrease in β deformation with neutron number whereas the vibrational γ band

lies 135 keV lower in this nucleus compared to ^{186}Os , pointing to an increasing importance of the γ degree of freedom. Interestingly, the excitation energy of the $K^\pi = 10^+$ bandhead differs by only 5 keV in the two nuclei and also other features are rather similar: Both bandheads are mainly populated from the odd-spin states 11^+ and 13^+ , whereas $E2$ transitions between the even-spin members of the band carry the flux at higher spins. The decay out of the band occurs mainly via quadrupole transitions from the 14^+ and 12^+ states to the 12^+ and 10^+ members, respectively, of the gsb. Finally, the bandhead decays in both cases via an $E1$ transition to the $K^\pi = 9^-$ intrinsic state. Based on these similarities we propose the same configuration for the $K^\pi = 10^+$ band in ^{188}Os as had been assigned to the bands in $^{184,186}\text{Os}$, namely the $i_{13/2}$ Fermi-aligned neutron configuration $\nu\{11/2^+[615], 9/2^+[624]\}$. The occupation of the high- $j_{i_{13/2}}$ orbital coupled to high K leads to rotation around an axis tilted with respect to the principal axes of the prolate spheroidal nuclear shape and this type of band is therefore called the t band. This configuration assignment is further supported by the large alignment of about $9\hbar$ observed for the yrast sequence in $^{184,186,188}\text{Os}$ as shown in Fig. 10.

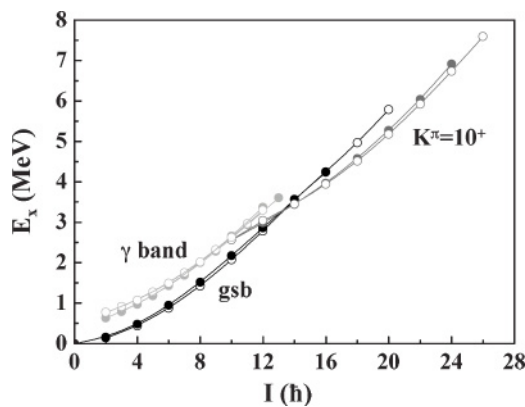


FIG. 9. Comparison between the ground-state bands (gsb), the $K^\pi = 10^+$ bands, and the γ bands in ^{186}Os (open symbols) and ^{188}Os (filled symbols).

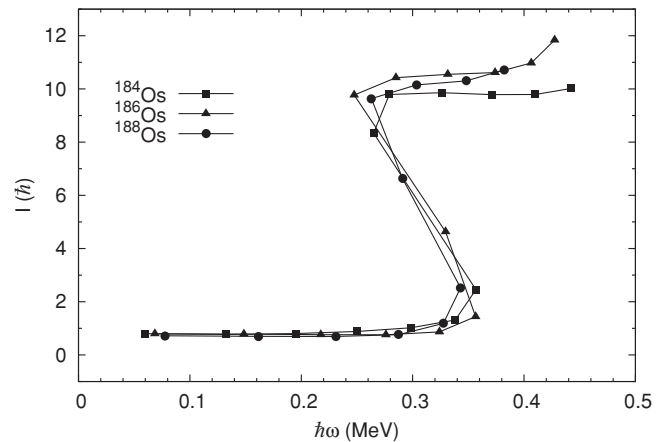


FIG. 10. Alignment plot for the gsb-t band sequences in ^{184}Os (squares), ^{186}Os (triangles), and ^{188}Os (circles).

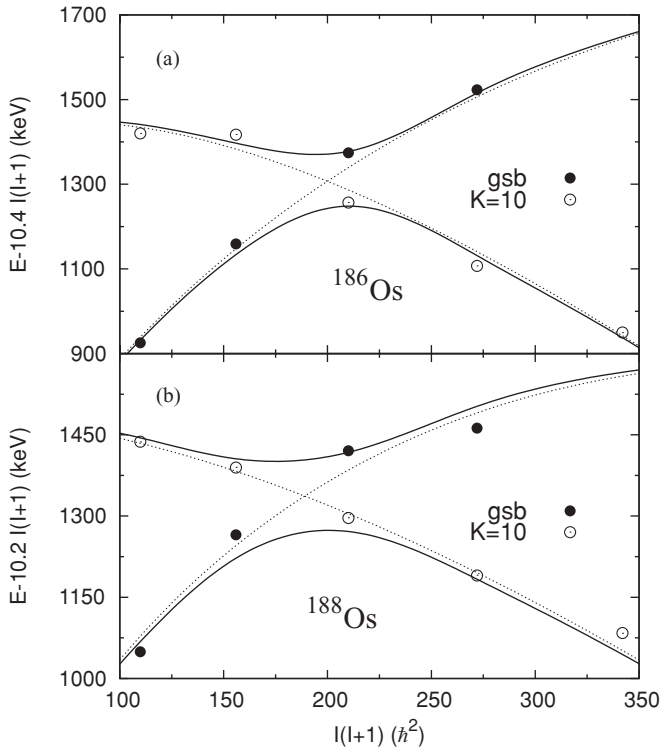


FIG. 11. Experimental yrast and yrare levels within the ground-state band (filled circles) and the tilted $K^\pi = 10^+$ band (empty circles). The dashed lines indicate the unperturbed bands and the solid lines the yrast and yrare bands obtained in the two-band-mixing fit.

The crossing between the gsb and the t band occurs around spin $12^+ - 14^+$ in both nuclei (see Fig. 9). The interaction between the two bands has been studied within the two-band-mixing model employed already in our previous work on the Dy isotopes [13]. A constant interaction strength $|V|$ is determined from a χ^2 fit of the unperturbed bands, which are parametrized with a variable moment of inertia [19]. The results are summarized in Table II and illustrated in Fig. 11.

The interaction strengths of 49(2) and 59(2) keV obtained for ^{184}Os and ^{186}Os , respectively, correspond to the maximum values allowed within the model and have therefore to be

TABLE II. Results of the two-band-mixing calculations for the interaction between the ground-state band and the $K^\pi = 10^+$ band in $^{184,186,188}\text{Os}$.

	$ V $ (keV)	\mathcal{J}^0 ($\hbar^2 \text{MeV}^{-1}$)	C ($\hbar^{-4} \text{MeV}^3$)	E^0 (MeV)
^{184}Os				
gsb	49(2)	19.4	0.003	0.00
t band		42.0	0.002	1.23
^{186}Os				
gsb	59(2)	21.7	0.005	0.10
t band		31.0	0.001	1.30
^{188}Os				
gsb	31(2)	19.3	0.003	0.26
t band		47.8	0.003	1.48

considered with caution. Although the value for ^{186}Os is in agreement with the value obtained by Wheldon *et al.* [8] for this nucleus, Shizuma *et al.* [20] determined an interaction strength of only 35 keV for ^{184}Os , much smaller than the value of 49(2) keV obtained in our analysis of this nucleus. However, the value of 35 keV for the gsb-t band interaction strength was obtained from a three-band-mixing calculation considering also the Stockholm band observed in ^{184}Os [20].

Very recently, Walker [21] analyzed the first band crossing in a series of well-deformed nuclei and deduced interaction strengths on the basis of the intensities of the four inter- and intraband $E2$ transitions in the crossing region. For ^{184}Os he obtained a value of $|V| = 44.6(4)$ keV, which is close to the one we obtained in our two-band-mixing fit.

B. High- K multiquasiparticle states

Besides the already known negative-parity 5^- , 7^- , and 9^- intrinsic states, which are based on two-neutron configurations including the $i_{13/2}$ orbital, a number of high- K states have been established for the first time in the present work. At positive parity these are the 10^+ bandhead of the $K^\pi = 10^+$ t band, the 14^+ level at 3472 keV (33 keV above the 14^+ yrast state), and the 16^+ and 18^+ states at 3735 and 4258 keV, respectively, which form the yrast line. At negative parity the 10^- (2145 keV) and 15^- (3414 keV) states are yrast while the 13^- level at 3094 keV lies 34 keV above the yrast line. For the 10^+ state we propose the $\nu\{11/2^+[615], 9/2^+[624]\}$ configuration in analogy to the $K^\pi = 10^+$ band in ^{186}Os as discussed already. The isomeric 10^- level [$\tau = 17.7(2)$ ns] at an excitation energy of 2145 keV is the only other among the newly identified high- K states that can be built with only two quasiparticles and we suggest the neutron configuration $\nu\{11/2^+[615], 9/2^-[505]\}$ involving a $h_{9/2}$ neutron in addition to the one in the $i_{13/2}$ shell for this level. Such a 10^- intrinsic state has not been observed in the lighter Os isotopes but in both ^{190}Os as well as ^{192}Os isomeric 10^- states have been identified. In ^{190}Os it lies at an excitation energy of 1705 keV and has a half-life of $T_{1/2} = 9.9$ min [22] and in ^{192}Os the excitation energy is 2015 keV and $T_{1/2} = 5.9$ s [23,24]. In both cases the two quasineutron $\nu\{11/2^+[615], 9/2^-[505]\}$ configuration was proposed by the authors. The reason for the much longer lifetime of these states in $^{190,192}\text{Os}$ might be that the 9^- state to which the 10^- level in ^{188}Os exclusively decays is not observed in the heavier isotopes, in agreement with the calculations discussed in the following, which indeed place the 9^- state above the 10^- level in $^{190,192}\text{Os}$. For the description of the other new intrinsic states with higher spin, four-quasiparticle configurations have to be considered including the $h_{9/2}$ and $p_{3/2}$ orbitals in addition to the $i_{13/2}$ shell. To help in the configuration assignment we have performed configuration-constrained multiquasiparticle PES calculations [4] with the non-axial-deformed Woods-Saxon potential [25]. The Lipkin-Nogami pairing is employed with the tracked blockings of the single-particle orbits that define the configuration [4]. The pairing strengths for the neutrons and protons have been adjusted to give the right odd-even mass differences as done in Ref. [26]. The calculated energies for the given configurations are compared to the experimental

TABLE III. Experimental and calculated excitation energies of multiquasiparticle states in $^{186,188}\text{Os}$.

K^π	Configuration	^{188}Os					^{186}Os	
		β_2	γ	β_4	E_{th}	E_{exp}	E_{th}^{a}	E_{exp}
10^+	$\nu\{11/2^+[615], 9/2^+[624]\}$	0.17	0°	-0.053	2153	2559	2338	2564
10^+	$\pi\{11/2^-[505], 9/2^-[514]\}$	0.16	-23°	-0.033	2013	—	—	—
14^+	$\nu\{11/2^+[615], 9/2^+[624], 9/2^-[505], -1/2^-[510]\}$	0.17	0°	-0.046	3618	3472	—	—
14^+	$\nu\{11/2^+[615], 9/2^+[624], 7/2^-[503], 1/2^-[510]\}$	0.18	0°	-0.054	3500	—	—	—
15^+	$\nu\{11/2^+[615], 9/2^+[624], 7/2^-[503], 3/2^-[512]\}$	0.18	6°	-0.055	3413	—	3390	3732
16^+	$\nu\{11/2^+[615], 9/2^+[624], 9/2^-[505], 3/2^-[512]\}$	0.17	0°	-0.048	3599	3735	—	—
18^+	$\nu\{11/2^+[615], 9/2^+[624], 9/2^-[505], 7/2^-[503]\}$	0.18	-16°	-0.048	3568	4258	4286	4496
5^-	$\nu\{11/2^+[615], -1/2^-[510]\}$	0.18	0°	-0.058	1777	1669	1707	1629
7^-	$\nu\{11/2^+[615], 3/2^-[512]\}$	0.18	0°	-0.060	1741	1772	1855	1775
9^-	$\nu\{11/2^+[615], 7/2^-[503]\}$	0.18	0°	-0.058	1752	2056	1828	2166
10^-	$\nu\{11/2^+[615], 9/2^-[505]\}$	0.17	22°	-0.044	2011	2145	—	—
13^-	$\nu\{11/2^+[615], 9/2^-[505], 7/2^-[503], -1/2^-[510]\}$	0.17	12°	-0.049	3322	3094	—	—
15^-	$\nu\{11/2^+[615], 9/2^-[505], 7/2^-[503], 3/2^-[512]\}$	0.17	0°	-0.050	3375	3414	—	—
15^-	$\nu\{11/2^+[615], -1/2^-[510]\} \otimes$ $\pi\{11/2^-[505], 9/2^-[514]\}$	0.16	-23°	-0.034	4007	3414	—	—
18^-	$\nu\{11/2^+[615], 9/2^+[624]\} \otimes$ $\pi\{11/2^-[505], 5/2^+[402]\}$	0.19	0°	-0.050	6064	—	4696	5027

^aFrom Reference [8].

excitation energies of the observed high- K states in Table III. Included in this table for comparison are also the experimental and calculated energies for the same configurations in ^{186}Os (taken from Ref. [8]). Note that the present calculations do not include the residual spin-spin interactions, which typically shift the calculated energies by ~ 100 keV, with favored configurations (such as particles with spins antiparallel and unlike particles with spins parallel) being shifted to lower energies and unfavored couplings pushed to higher energies. By taking this shift into account qualitatively the agreement between the calculations and the experimental energies is generally satisfactory and in many cases even very good in support of the assignments made. The calculated shape parameters γ and $\beta_{2,4}$ are included in Table III, too. The quadrupole deformation β_2 stays nearly constant over the whole considered spin range ($\beta_2 = 0.16\text{--}0.19$) and the hexadecapole shape parameter β_4 shows variations between -0.060 and -0.033 . Most of the intrinsic states under study have axially symmetric shapes, some of them with well-defined minima, for example the 0^+ and 14_1^+ states, with others being very soft in the γ degree of freedom (e.g., the 10^+ and 14_2^+ states). The 15^+ , 18^+ , 10^- , 13^- , and 15^- states however show triaxial minima. As an illustration the calculated PES values for the ground state and the second 14^+ , and the 18^+ states are shown in Fig. 12.

C. Hindrances of intrinsic-state decays

Among the newly identified high- K states the 14^+ level has a strong highly forbidden decay branch to the 12^+ member of the ground-state band. To compare the strength of this transition to decays in the neighboring Os isotopes, we estimate its hindrance per degree of K -forbiddenness, or reduced

hindrance, according to

$$f_v = (T_\gamma/T_W)^{1/\nu},$$

where T_γ is the partial γ -ray half-life and T_W is the Weisskopf single-particle estimate. The change in K for this transition is difficult to establish because it populates the gsb in the band-crossing region with the t band where mixing effects are to be expected. Assuming a half-life limit of 2 ns for the 14^+ state we obtain reduced hindrance limits of $f_v < 1.3$

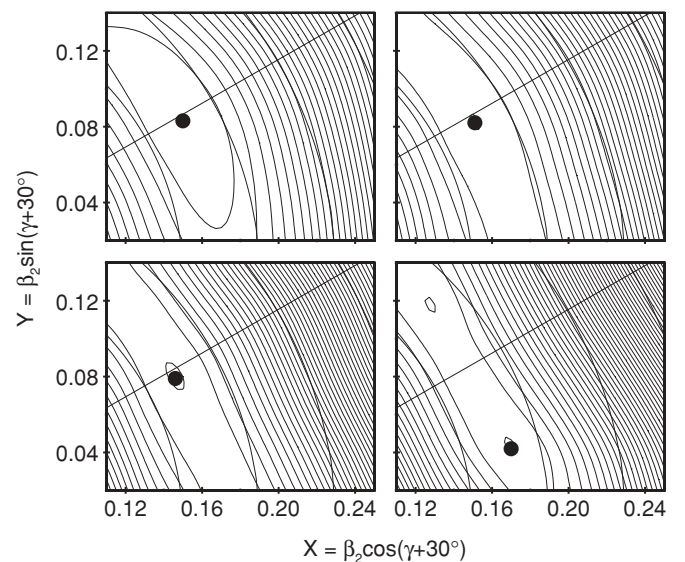


FIG. 12. Calculated potential energy surfaces for the ground state (top left), the 10^+ state (top right), the second 14^+ state (bottom left), and the 18^+ state (bottom right).

and $f_v < 2.2$ for $\Delta K = 14$ and $\Delta K = 4$, respectively. These values are in the same range as the ones obtained for the decays of the $K^\pi = 16^+$ state in ^{182}Os and $K^\pi = 20^+$ in ^{184}Os to the respective ground-state bands. In those cases, however, the multi-quasiparticle states lie quite high above the yrast line and statistical K mixing might contribute to the reduction of the hindrance for these transitions. Note that for the 20^+ level in ^{184}Os PES calculations do not predict triaxial deformation [3]. In the decay of the $K^\pi = (18^-)$ isomer in ^{184}Os three K -forbidden γ transitions are observed with f_v values between 3.7 and 8.2 [6]. These values follow nicely the correlation between f_v values and relative excitation energy of the K isomers established in Ref. [2] and can be explained within the statistical model. In the case of the $K^\pi = 25^+$ isomer in ^{182}Os [7] both statistical mixing as well as triaxiality as obtained in Ref. [4] may contribute to the experimentally observed low hindrance for the $\Delta K = 25$ decay to the gsb.

The situation is different for both the $K^\pi = 18^+$ state decaying to the t band in ^{186}Os ($f_v < 1.2$) and the $K^\pi = 14^+$ level in ^{188}Os with the forbidden decay to the gsb just discussed. The 18^+ state in ^{186}Os is yrast by 10 keV and the 14^+ level in ^{188}Os lies only 33 keV above the 14^+ member of the t band, which marks the yrast line at this spin. In these cases statistical K mixing can be excluded and γ softness or triaxial deformation seem to be the most probable explanations for the low hindrances of these K -forbidden transitions. For ^{186}Os PES calculations have been performed and indeed indicate a triaxial deformation of the 18^+ level [8]. Our present multi-quasiparticle PES calculations give very similar energies for two different four-quasineutron configurations for the 14^+ state, making a configuration assignment for this level exclusively based on the excitation energy difficult. However, since the low reduced hindrance for the decay of the experimental 14^+ state at 3472 keV to the gsb determined as discussed previously is explained in

a more natural way if its PES is very γ soft as observed for the second 14^+ state (compare Fig. 12), we propose the $\nu\{11/2^+[615], 9/2^+[624], 9/2^-[505], -1/2^-[510]\}$ configuration for it based on the calculated energy surfaces.

V. SUMMARY

The nucleus ^{188}Os has been populated in the incomplete fusion reaction $^7\text{Li} + ^{186}\text{W}$ by allowing for the construction of its excitation scheme up to spin (24^+). A $K^\pi = 10^+$ band has been established and its crossing with the ground-state band has been studied. A number of new intrinsic high- K states have been identified and on top of two of them, $K^\pi = 7^-$ and $K^\pi = 10^-$, regular two-quasiparticle bands have been observed. Two of the high- K states with spins of 16^+ and 18^+ are yrast and a third, the 14^+ level, lies only 33 keV above the yrast line. Based on the low reduced hindrances obtained for the decay of this 14^+ state to the ground-state band we propose the neutron configuration $\nu\{11/2^+[615], 9/2^+[624], 9/2^-[505], -1/2^-[510]\}$ for which the PES is very soft in the γ degree of freedom. The new experimental information extends the systematics of collective bands and intrinsic states in the even-even Os isotopes to the more neutron rich isotope ^{188}Os .

ACKNOWLEDGMENTS

The authors would like to thank Prof. Herbert Hübel from the University of Bonn for providing the ^{186}W target. This work was supported by the Spanish Ministerio de Educación y Ciencia within the programa Ramón y Cajal and research Project Nos. FPA2005-00696 and FPA2007-66069 and by the Spanish Consolider-Ingenio 2010 Program CPAN (CSD2007-00042).

-
- [1] P. Walker and G. Dracoulis, *Nature (London)* **399**, 35 (1999).
 - [2] P. M. Walker *et al.*, *Phys. Lett.* **B408**, 42 (1997).
 - [3] C. Wheldon, G. D. Dracoulis, R. T. Newman, P. M. Walker, C. J. Pearson, A. P. Byrne, A. M. Baxter, S. Bayer, T. Kibdi, T. R. McGoram, S. M. Mullins, and F. R. Xu, *Nucl. Phys.* **A699**, 415 (2002).
 - [4] F. R. Xu, P. M. Walker, J. A. Sheikh, and R. Wyss, *Phys. Lett.* **B435**, 257 (1998).
 - [5] C. Wheldon, P. M. Walker, P. H. Regan, T. Saito, N. Hashimoto, G. Sletten, and F. R. Xu, *Phys. Rev. C* **59**, R2334 (1999).
 - [6] T. Shizuma *et al.*, *Phys. Rev. C* **65**, 064310 (2002).
 - [7] P. Chowdhury *et al.*, *Nucl. Phys.* **A485**, 136 (1988).
 - [8] C. Wheldon *et al.*, *Nucl. Phys.* **A652**, 103 (1999).
 - [9] J. W. Yates, J. C. Cunnane, R. Hochele, and P. J. Daly, *Nucl. Phys.* **A222**, 301 (1974).
 - [10] R. A. Warner *et al.*, *Phys. Rev. Lett.* **31**, 835 (1973).
 - [11] T. Yamazaki and K. Nishiyama, *Nucl. Phys.* **A209**, 153 (1973).
 - [12] C. Y. Wu *et al.*, *Nucl. Phys.* **A607**, 178 (1996).
 - [13] A. Jungclaus *et al.*, *Phys. Rev. C* **66**, 014312 (2002).
 - [14] A. Jungclaus *et al.*, *Phys. Rev. C* **67**, 034302 (2003).
 - [15] A. Jungclaus *et al.*, *Phys. Rev. C* **77**, 024310 (2008).
 - [16] V. Modamio *et al.* (in preparation).
 - [17] T. A. Shibata, H. Nakayama, T. Numao, and T. Yamazaki, *Nucl. Phys.* **A312**, 115 (1978).
 - [18] Zs. Podolyak *et al.*, *Int. J. Mod. Phys. E* **13**, 123 (2004); S. Mohammadi *et al.*, *ibid.* **15**, 1797 (2006).
 - [19] M. A. J. Mariscotti, G. Scharff-Goldhaber, and B. Buck, *Phys. Rev.* **178**, 1864 (1969).
 - [20] T. Shizuma *et al.*, *Phys. Lett.* **B442**, 53 (1998).
 - [21] P. M. Walker, *J. Phys. G* **34**, 123 (2007).
 - [22] G. Scharff-Goldhaber, D. E. Alburger, G. Harbottle, and M. McKeown, *Phys. Rev.* **111**, 3 (1958).
 - [23] J. Blachot, E. Monnard, and A. Moussa, *Compt. Rend.* **261**, 1835 (1965).
 - [24] A. Pakkanen and D. W. Heikkinen, *Phys. Fenn.* **8**, 345 (1973).
 - [25] W. Nazarewicz *et al.*, *Nucl. Phys.* **A435**, 397 (1985).
 - [26] F. R. Xu, R. Wyss, and P. M. Walker, *Phys. Rev. C* **60**, 051301 (1999).